Experimental Study and Modeling of Lapping Using Abrasive Grits with Mixed Sizes

Chunhui Chung
Research Fellow
Department of Mechanical Engineering,
National Chiao Tung University,
Hsinchu, Taiwan 30010

Chad S. Korach
Assistant Professor

Imin Kao[1]
Professor
e-mail: kao@mal.eng.sunysb.edu

Department of Mechanical
Engineering,
Stony Brook University,
Stony Brook, NY 11794-2300

In this paper, the lapping process of wafer surfaces is studied with experiments and contact modeling of surface roughness. In order to improve the performance of the lapping processes, effects of mixed abrasive grits in the slurry of the free abrasive machining (FAM) process are studied using a single-sided wafer-lapping machine. Under the same slurry density, a parametric experimental study employing different mixing ratios of large and small abrasive grits and various normal loadings on the wafer surface applied through a jig is conducted. Observations and measurements of the total amount of material removed, material removal rate, surface roughness, and relative angular velocity are presented as a function of various mixing ratios and loadings and discussed in the paper. The experiments show that the 1:1 mixing ratio of abrasives removes more material than other mixing ratios under the same conditions, with a slightly higher surface roughness. Modeling of the mixed abrasive particle distributions correspondingly indicates that the roughness trend is due to the abrasive size distribution and the particle contact mechanics. The results of this study can provide a good reference to the FAM processes that practitioners use today by exploiting different abrasive mixing ratios in slurry and normal loadings in the manufacturing processes. [DOI: 10.1115/1.4004137]

1 Introduction

Wafers made of materials such as silicon, III-V and II-VI compounds, and optoelectronic materials, require a high-degree of surface quality in order to increase the yield in micro-electronics fabrication to produce integrated circuits and devices. Due to the reduction of feature size in micro-electronics fabrication, the requirements of the wafer surface qualities, such as the commonly defined site flatness, nanotopography, total thickness variation, and warp [1], become more and more stringent. To meet such requirements, the wafer manufacturing processes of brittle semiconductor materials, including slicing, lapping, grinding, and polishing have been continually improved. Following Moore's law, the international technology roadmap of semiconductors indicates that the 450 mm wafer will be in production in 2012 [2] to keep the trend of cost reduction. Many analyses and discussions have started to focus on the next generation wafer size [3–8]. With the agreement of Intel, Samsung Electronics, and Taiwanese Semiconductor Manufacturing Company Limited (TSMC) at the 450 mm wafer manufacturing transition [9], the next increase of wafer size is inevitable. With such increase, it is more difficult to achieve the requirements of wafer surface quality. Therefore, the advance of the machining processes such as wiresawing, lapping, and grinding is important.

Lapping has been a standard surface finishing process for glass products and semiconductor wafers for a long time. Lapping, by virtue of using third-body free abrasive for removing materials from substrate surface, belongs to the category of the free abrasive machining process, which is the same as slurry wiresaw slicing [10–12]. Although most research attributes the brittle material removal of lapping to indentation cracking models [13–17], the actual mechanism is more complicated [18–20]. Aside from the mechanical properties of the workpiece and lapping plate, the distribution of abrasives, dynamic indentation cracking, motion of the abrasive grits and the ductile-regime machining [21] also complicate the analysis of the lapping mechanism.

Lapping and grinding are both postslicing wafer surface finishing processes. Because of their advantages and disadvantages, one or both of them are utilized in the manufacturing process [22,23]. It is not clear which one will be favorable or employed in the 450 mm wafer industry. However, lapping is capable of removing warp efficiently until the invention of simultaneous double-sided grinding [23,24]. In this paper, an experimental study and modeling of the surface roughness generated from lapping with a mixed abrasive slurry provides information on the influence of abrasive distributions in lapping.

Past research has emphasized the importance of abrasive size distribution in modeling; however, few have studied the change of the distribution of abrasive grit sizes. Bhagavat, et al. [1] is probably the first and the only one to study such topic. Their results showed that the mixed abrasives (for example, mixing F-400 and F-600 SiC) have higher material removal rate than the single-sized abrasives (for example, only F-400 SiC abrasives). However, their experiments discussed one mixing ratio of the abrasives, and the concentration of mixed abrasive slurries were different from that of the single-sized abrasives slurry. To study the influence of the change of abrasive distribution in lapping, experiments with different abrasive distributions and constant slurry concentration are necessary.

In this study, experiments were conducted by mixing two different sizes of SiC powders: F-400 and F-600. Five different mixing ratios of the abrasives were employed, with the ratio of the total mass of abrasives to the volume of carrier fluid (de-ionized (DI) water) being kept the same. The results show that the 50% mixing ratio (1:1) of the two different abrasives have the highest material removal rate (MRR), with a slightly higher surface roughness. In addition, the material removal rate is nearly proportional to the normal loading. The surface roughness, however, depends on the distribution of mixed abrasive grits but not the total loading. This is comparable to results presented in the literature [14,15]. A model of surface roughness based on particle contact depth was utilized to compare the effects of different mixing ratios. The roughness and penetration depth in lapping have been modeled by the Hertzian formulation [25,26], as well as the statistical nature of the contact using probability functions [17,18,27]. The particle distribution nonuniformity (standard deviation) has
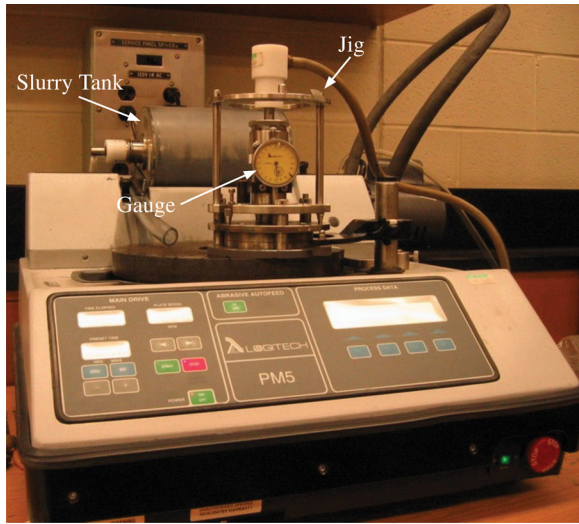

Fig. 1 Logitech PM5 lapping machine, employed to conduct experiments in this paper

been found to correlate with the MRR in lapping [28], where for a large variation in particle size led to an increased MRR. Here, the contact depth is obtained by the Hertzian formulation of Cook [26] and extended to a roughness analysis using two particle distributions. This model considers the particle size effect on active abrasive grits, the abrasive size distributions, and the applied load, to provide a correlation with the experiments using the process parameters.

2 Experimental Setup

Logitech PM5 one-sided lapping machine, as shown in Fig. 1, was employed in this experimental study. A PP6GT jig was used to hold the silicon wafer, which was mounted on glass plate by wax. The dial gauge mounted on the jig provides real-time measurement of the material removal depth during the lapping operation. In addition, the jig provides a constant normal load on the wafer during the machining process. All wafers used in the experiments are 3-in. lapped Si(111) wafers with initial root-mean-square (rms) surface roughness of 0.4 μm, purchased from Virginia semiconductor.

Two different grades of silicon carbide powders, F-400 and F-600, were used in the experiments. The median sizes of F-400 and F-600 powders are 17.3 μm and 9.3 μm, respectively[2]. Table 1 shows the Federation of European Producers of Abrasives (FEPA) *Grading Chart* of these two abrasive grits. DI water was chosen as the carrier fluid. In order to study the different distribution of abrasives in slurry, the ratio of the weight of abrasives to the weight of carrier fluid, C, was kept at a constant value of 0.154. Five different ratios of the weight of F-400 powder, W_{400}, to the total weight of abrasives, W_{total}, were employed in the experiments to study the effect of different distribution of abrasives in the lapping process. The ratios are $W_{400}/W_{\text{total}} = 0, \frac{1}{4}, \frac{1}{2}, \frac{3}{4}$, and 1.

During the experiments, the angular velocity of the cast iron lapping plate was kept at 70 rpm. The recording of experimental data was started after 3 min of machining in order to avoid the influence of initial surface roughness on the initial material removal. The material removal depth and the angular velocity of the jig were recorded every 5 min. Every experiment lasted for 30 min. Two different loadings, 2.3 and 4.1 kg (5 and 9 lb), were applied on the jig. Therefore, there were ten different settings, including five abrasive distributions each with two loadings. For each setting, six experiments were conducted.

[2]According to different measurement, there are different results for the distribution of abrasive grits [29]. In this paper, we follow the FEPA grading chart.

Table 1 FEPA Grading Chart of F-400 and F-600 SiC powders (micrometer)

SiC powder	D3%	D50%	D94%
FEPA F-400	32	17.3 ± 1.5	8
FEPA F-600	19	9.3 ± 1	3

After lapping, the wafer was cleaned by de-ionized water, and the wax was melted to remove the silicon wafer from the glass plate. Surface morphology was examined with a Keyence optical microscope, and the surface roughness was measured with an XP2 profilometer at eight randomly selected locations. Each surface roughness scan is 2 mm in length, which is much larger than the size of fractures on the wafer surface.

3 Results and Analysis

3.1 Material Removal Depth. The reduction of the wafer thickness during the lapping process was measured in real-time by the dial gauge every 5 min. in order to record the history of the material removal rate under different loadings and distribution of abrasive grits. Figure 2 plots the results of experiments.

There are two important observations in the two graphs. First, when $W_{400}/W_{\text{total}} = 0.5$, it has the highest material removal rate regardless of the loading being 2.3 or 4.1 kg. When $W_{400}/W_{\text{total}} = 0$, with only the F-600 grits in the slurry, the material removal rate is always the lowest. The other three distribution ratios of abrasives have similar material removal rates. However,
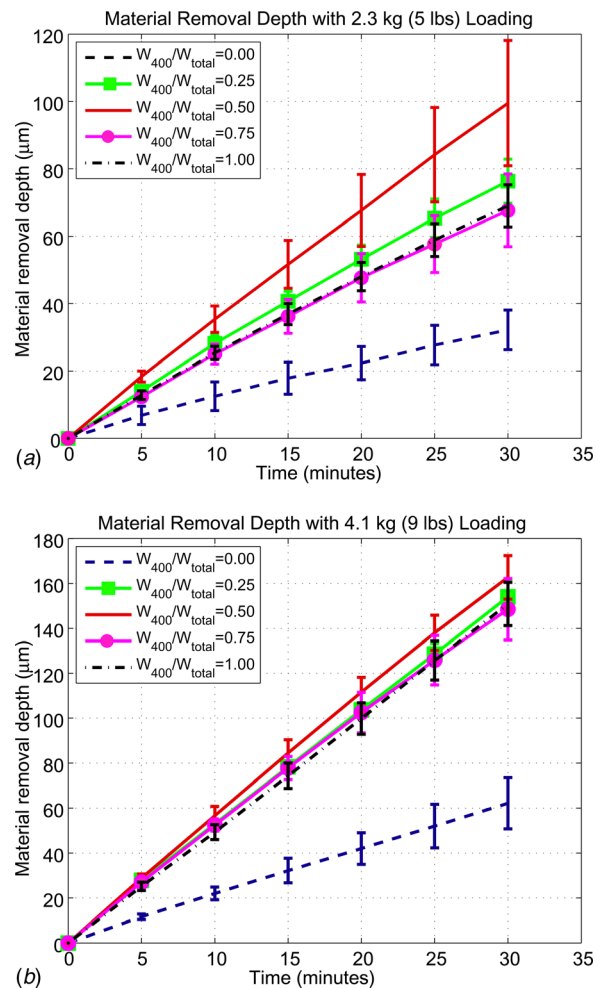

Fig. 2 Depth of the material removal with (a) 2.3-kg and (b) 4.1-kg loadings in lapping
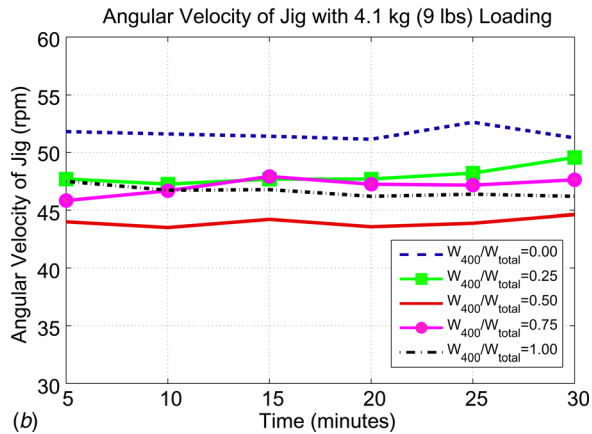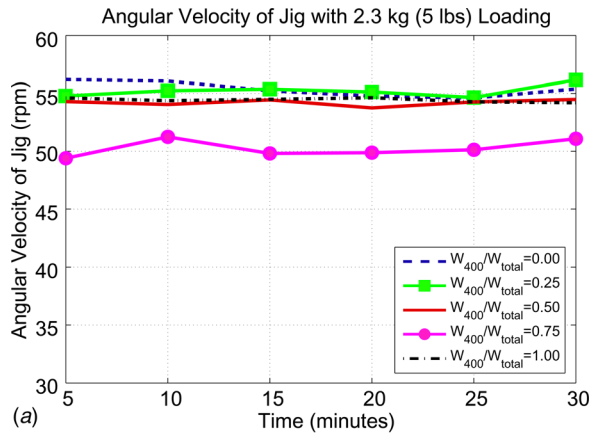
Fig. 3 Angular velocity of jig with the (a) 2.3-kg and (b) 4.1-kg loadings during lapping

Fig. 4 Average rms surface roughness after lapping. The unit is in micron.

the material removal rate with 50% mixing ratio at the loading of 4.1 kg is not more prominent than the case with the loading of 2.3 kg. The contrast can be observed from Fig. 2. Furthermore, the material removal rate is always higher under 4.1 kg loading with the same mixing ratio of abrasive grits, as expected.

3.2 Angular Velocity of the Jig. The angular velocity of the jig is a passive parameter of the lapping experiments and cannot be controlled independent of the speed of the lapping plate. The results were also recorded every 5 min during the experiments and plotted in Fig. 3 to show the history of the angular speed of the jig.

The figures show that the angular velocities of the jig vary within a small range. The jig has higher angular velocity with the lower loading of 2.3 kg than that with the higher loading. This means that the relative angular velocity between the jig and the lapping plate, which has a constant angular velocity of 70 rpm during the experiments, is lower at the 2.3 kg loading. However, there is no significant correlation between the angular velocity of the jig and the other parameters, such as material removal rate or surface roughness.

3.3 Surface Roughness. One purpose of lapping is to flatten the wafer after slicing for better surface quality. Although the chemical–mechanical polishing is the final process to achieve the mirrorlike wafer surface finish, the surface topography after lapping is very important. Figure 4 shows the average rms surface roughness after lapping, measured by the XP2 profilometer with a diamond probe. The figure shows that the surface roughness does not correlate significantly to the increase of loading, as presented in the literature [14,15]. However, the different ratios of the mixed abrasive grits result in different surface roughness, with the half–
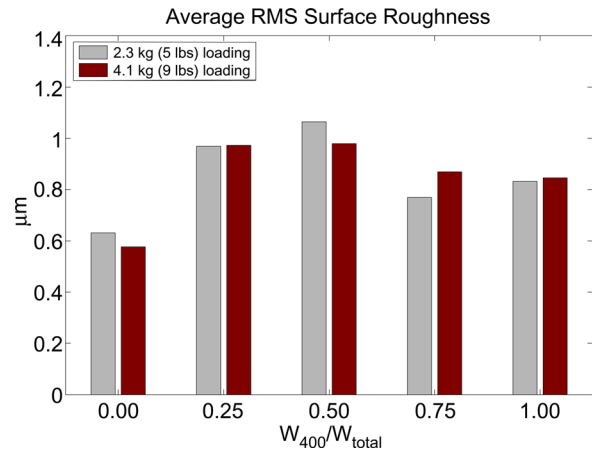
half mixed abrasive slurry having the highest surface roughness under the same loading.

Comparing to Fig. 2, we found that the higher material removal rate in the machining operation usually is accompanied by a higher surface roughness. This is intuitive. The results here illustrate that the change of the distribution of abrasive grits will affect material removal rate and surface roughness.

3.4 Surface Morphology. The surfaces of lapped wafers were examined by optical microscope. Features and evidence of cracks, indentation marks, and scratches can be seen on the lapped surface under the microscope. These surface features show the complicated machining mechanisms to shape the surface. Figure 5 shows typical surface morphology of silicon wafer after lapping conducted in this study.

4 Surface Roughness Model for Mixed Abrasive Lapping

The roughness resulting from the mixed abrasive lapping process is modeled by the roughness contribution resulting from each abrasive powder in the mixed distribution. This is accomplished by a rule of mixtures of the mass percentage of each abrasive constituent in the slurry. By modeling the roughness in this manner, each abrasive particle size can be considered separately, though the contact interaction effect of each particle size on the other will be considered within individual models. Take the roughness generated by the F-400 and F-600 abrasives on the silicon substrate as
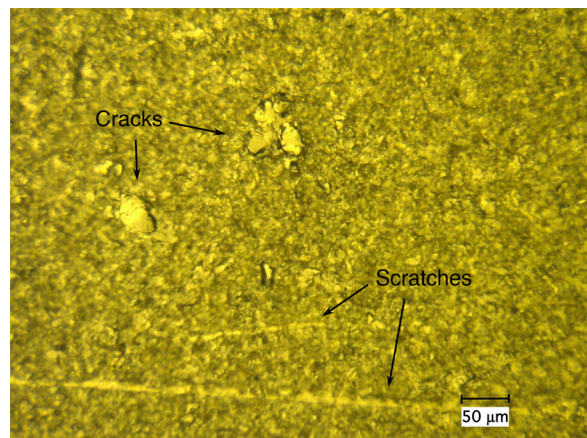

Fig. 5 Typical surface morphology of lapped wafer surface. The scale bar is 50 μm.

R_s^{400} and R_s^{600}, respectively, then combining in a rule of mixtures yields the relationship for the total silicon substrate roughness

$$R_s = \chi R_s^{400} + (1 - \chi)R_s^{600} \qquad (1)$$

where the weight percent ratio is $\chi = W_{400}/(W_{400} + W_{600})$.

To model the roughness of the lapping process, the mechanics between abrasive particles and the silicon substrate are modeled as spherical particles penetrating the substrate with a constant load. Abrasion is assumed as the dominating material removal mechanism. The general equation for the roughness is based on the penetration depth of an abrasive particle into the silicon substrate. The framework has been presented by Brown et al. [25] and later by Cook [26], and has been applied to glass polishing, super polishing of metals, and ductile grinding of brittle materials. Here, we extend the model framework to consider mixed abrasive distribution effects on the resulting substrate roughness from mixed abrasive lapping. The model treats the abrasives as spherical particles, where in reality the particles will have sharp asperities that may increase contact depth (roughness) in the model. This assumption was made for simplicity and will be addressed in the future. If a concentration of k spherical abrasive particles (with diameter of ϕ) are in contact with a nominal pressure per particle (p), the roughness for a specific distribution (R_s^i) is represented by the surface penetration

$$R_s^i = \frac{3\phi}{4}\left(\frac{p}{2kE_r}\right)^{2/3} \qquad (2)$$

where p is the nominal pressure of the wafer-platen interface and is determined by dividing the applied load by the nominal wafer area (76.2 mm diameter wafer), and i indicates the abrasive powder (either F-400 or F-600). The reduced modulus of the contact (E_r) is given by

$$\frac{1}{E_r} = \frac{1 - \nu_p^2}{E_p} + \frac{1 - \nu_s^2}{E_s} \qquad (3)$$

where E_s is the Si(111) substrate elastic modulus (=190 GPa) with the Poisson ratio of $\nu_s = 0.26$, and the SiC particle elastic modulus is $E_p = 415$ GPa, with $\nu_p = 0.16$. These values yield a reduced modulus of $E_r = 138$ GPa. Since the slurry is composed of mixed abrasives, each particle size will contribute to the overall contact and hence roughness of the substrate. Equation (2) is applied to both particle sizes, F-400 and F-600, taking the contributions into consideration separately. The diameters are taken as one standard deviation from the mean, 15.8 and 10.3 μm for F-400 and F-600, respectively. From Eq. (2), the contact is governed by the concentration factor k, where as k becomes small, the roughness increases, due to an increase in the per particle contact load.

The interaction between the F-400 and F-600 particles will affect the resulting individual abrasive powder roughness on the silicon substrate. For a single abrasive case, the general relationship in Eq. (2) shows that as particle concentration decreases there will be a subsequent increase in roughness, due to the per particle load increase, which increases surface penetration. The model predicts a singularity in roughness as $k \to 0$, where in reality there will be a geometric limit to the roughness based on the particle size and the contact with the substrate and platen, which is one-half the particle diameter, or $R_{s,\text{limit}} = 0.5\phi$. For the abrasive particles (either F-400 or F-600), this limit would occur at $k = 5.86 \times 10^{-8}$ for $P = 40.1$ N (4.1 kg), and $k = 3.25 \times 10^{-8}$ for $P = 22.3$ N (2.27 kg). However, the limiting value of roughness for the particle distributions is never reached for the mixed abrasive cases, due to the presence of the second particle distribution in the slurry. For the F-400 case there would be a contact interaction effect beginning at a critical concentration of the F-600 par-

ticles, where large diameter particles present in the F-600 distribution begin to make contact. This phenomenon occurs up to a limit based on the F-600 particles reaching full concentration and hence limiting the F-400 particle surface penetration. The penetration limit of the F-400 particles is determined by considering the maximum penetration of the F-600 particles at full concentration in addition to the difference between the F-400 and F-600 particle radius, and is given by

$$R_S^{400}\big|_{\text{limit}} = \frac{3\phi_{600}}{4}\left(\frac{p}{2k_{\max}E_r}\right)^{2/3} + \frac{1}{2}(\phi_{400} - \phi_{600}) \qquad (4)$$

In the case of the F-600 particles, the resulting roughness is affected by the F-400 particle concentration, which for increasing concentration will effectively replace the F-600 particle contacts, limiting the F-600 particles to only the largest in the distribution to contribute to the penetration.

The model for the F-400 roughness contribution during mixed abrasive lapping is written as

$$R_s^{400} = \frac{3\phi_{400}}{4}\left(\frac{p}{2k_{400}E_r}\right)^{2/3}, \quad k^* \le k_{400} \le k_{\max} \qquad (5)$$

$$R_s^{400} = \frac{3\phi_{400}^{\text{eff}}}{4}\left(\frac{p}{2(k_{400} + \beta)E_r}\right)^{2/3}, \quad 0 \le k_{400} \le k^* \qquad (6)$$

The concentration $k*$ represents the critical point, where F-600 particles of large enough diameter will begin to contribute to the load bearing and is represented by

$$k^* = k_{\max} \cdot \chi\big|_{\%\text{cr}} \qquad (7)$$

where $\chi\big|_{\%\text{cr}}$ is a percentage based on the F-600 particle distribution shape (Fig. 6). Assuming a normalized linear particle distribution with a maximum at 9.3 μm and a value of 19 μm at 3% of the distribution, the slope of this linear distribution in Fig. 6 between these two points is found to be $-0.1\%/\mu$m. A critical particle diameter (15.8 μm) is assumed for the F-600 distribution, above which it will contribute to the contact. This value is based on the F-400 particle distribution, and is determined by taking one standard deviation from the F-400 distribution mean value, i.e., 17.3–1.5 μm = 15.8 μm. When the number of F-600 particles greater than 15.8 μm is equivalent to 10% (%cr) of the total number of particle contacts (combined with the F-400 particles) a critical $\chi\big|_{\%\text{cr}}$ can be determined by
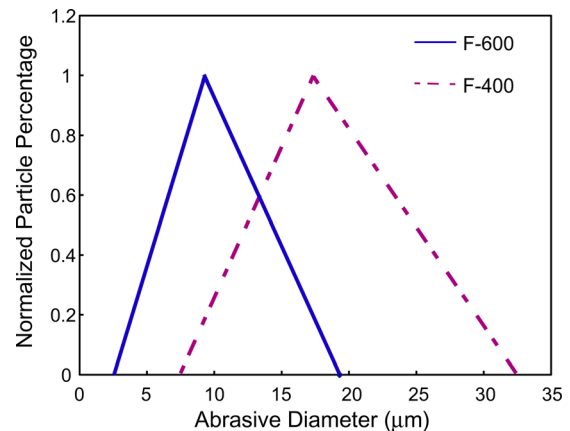

Fig. 6 Normalized linear distributions for FEPA F-400 and F-600 SiC powders, based on data in Table 2. The slope of the F-600 powder from the mean size to the maximum size is calculated as $-0.1\%/\mu$m. The tail portion of the F-600 distribution from 15.8 μm to the maximum is 7.3% of the total distribution volume.

$$\frac{(1-\chi)\alpha}{(1-\chi)\alpha + \chi} = \%cr \qquad (8)$$

where χ can vary between 0 and 1, and α is the ratio of the number of critical F-600 particles that could be in contact. The ratio α is determined by the slope above of the F-600 distribution and the intersection of the lower value of the F-400 distribution mean (15.8 μm) and the F-600 distribution, which occurs at $\alpha = 7.3\%$. The value of $\%cr = 10\%$ is an assumption and states that 10% of the F-600 particles which have a diameter size larger than 15.8 μm will contribute to the contact. It was found that the result of $\chi|_{\%cr}$ within the experimentally measured range of the mixing ratios had small variations in %cr around 10%. Equation (8) yields a value of $\chi|_{\%cr} = 0.4$. Thus, from Eq. (7), $k^* = 0.4\, k_{max}$, for the F-400 and F-600 mixed abrasive slurry. Between concentrations $k = 0$ to k^*, the R_s^{400} values follow Eq. (6). Since the maximum penetration of the F-400 distribution is given by Eq. (4), the roughness from the F-400 particle distribution will fall on a curve between $R_s^{400}|_{limit}$ and $R_s^{400}|_{k=k^*}$; the latter, which is the intercept with the R_s^{400} model between $k^* < k < k_{max}$, can be determined by Eq. (5) when $k = k^*$. Thus, the roughness between $0 < k < k^*$ is bound by the physical particle size limitation of the average F-400 particle and the critical concentration, where the F-600 particles begin to make a significant contribution to the load bearing, affecting the F-600 penetration depth. The R_s^{400} model in Eq. (6) is fit between these two points where ϕ_{400}^{eff} and β are constants. Physically, ϕ_{400}^{eff} represents the effective change in the particle diameter with the introduction of the F-600 particles, which will affect the penetration depth. The constant can be solved by

$$\phi_{400}^{eff} = \frac{4}{3} R_s^{400}\big|_{limit}\left(\frac{2\beta E_r}{p}\right)^{2/3} \qquad (9)$$

where $R_s^{400}|_{limit}$ is given by Eq. (4), and β represents a shift in the concentration to take into consideration the addition of the F-600 particles on the load bearing. The constant β can be computed by

$$\beta = 0.4 k_{max}\left[\frac{R_s^{400}|_{k^*}}{R_s^{400}|_{limit}}\right]^{3/2}\left(1 - \left[\frac{R_s^{400}|_{k^*}}{R_s^{400}|_{limit}}\right]^{3/2}\right)^{-1} \qquad (10)$$

which is a function of the maximum concentration factor (k_{max}) and the pressure, p. Combining the model in Eqs. (4), (5), (6), (9), and (10) piecewise continuously, there is a decrease in the F-400 roughness (R_s^{400}) from a maximum value at $k_{400} = 0$ to k^* and minimizing at k_{max} (Fig. 7). The decrease in R_s^{400} with increasing concentration k_{400} is expected; as the load per particle decreases, the particle penetration will then decrease. The critical concentration value is generated due to the particle distribution overlap and proximity of the average particle sizes. As the distribution overlap decreases to zero, i.e., the distributions separate, the critical point k^* will move towards $k_{400} = 0$. This is a direct result of the reduced interaction between the larger F-600 particles and the F-400 distribution penetration depth. In fact, when the distributions move closer, i.e., an increase in the overlap due to a small separation between the mean values, the maximum depth limit (Eq. (4)) which occurs at the low concentrations of F-400 will decrease; though k^* will increase due to a larger distribution overlap.

The model for the F-600 roughness contribution during mixed abrasive lapping is written as

$$R_s^{600} = \frac{3\phi_{600}^{eff}}{4}\left(\frac{p}{2 k_{max} E_r}\right)^{2/3}, \quad 0 \le k_{600} \le k_{max} \qquad (11)$$

where k_{600} is the volume concentration of the F-600 particles. Here, ϕ_{600}^{eff} is the effective particle diameter of the F-600 distribution and physically represents the effective increase in the particle size due to the introduction of F-400 load bearing particles.
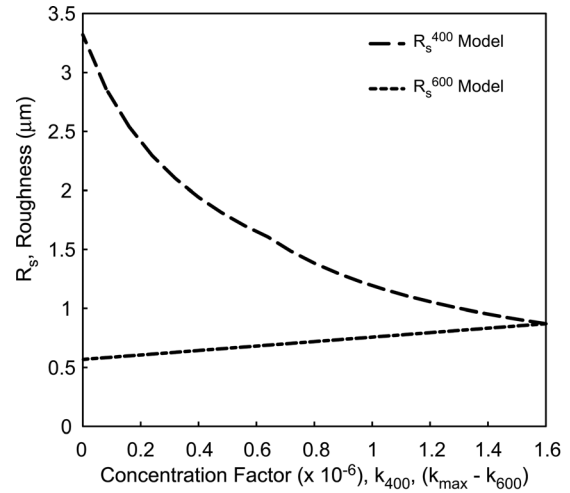

Fig. 7 Plot of individual roughness contributions from the F-400 and F-600 roughness models, as a function of the concentration factor k. For R_s^{400}, k is defined by k_{400}, though for R_s^{600}, k is defined by ($k_{max} - k_{600}$) to plot on the same axis. As abrasive concentration decreases (decrease in k) the roughness decreases for the models of both powders. F-400 is affected by the interaction of the F-600 abrasives beginning at a critical concentration $k^* = 0.4\, k_{max}$, and is the reason for the change in slope of the F-400 roughness curve at $k = 0.64 \times 10^{-6}$.

The particle concentration is held constant at k_{max}, since as k_{600} decreases, the F-600 particles will be replaced by the larger F-400 particles, keeping the concentration of particles in contact approximately constant. The F-400 interaction effect on the particle diameter is modeled to increase in a linear manner, therefore ϕ_{600}^{eff} is represented by

$$\phi_{600}^{eff} = (1-\chi)\phi_{600} + \chi\phi_{400} \qquad (12)$$

where $\phi_{600}^{eff} \to \phi_{400}$ as the percentage of F-400 increases, since the F-600 particles will not be the dominate contacts as $k_{600} \to 0$ and will effectively be limited by the F-400 particle size on the particle penetration depth, and hence roughness. Thus, $R_s^{600}|_{k=0} \to R_s^{400}|_{k=k_{max}}$ is a logical conclusion of the model (Fig. 7). The effect of the F-400 particle interaction on R_s^{600} will cause a decrease in the roughness parameter over the result of R_s^{600}, and provide an upper bound at the F-600 low concentrations. The F-600 distribution roughness increases as the concentration k_{600} decreases (Fig. 7) up to a limit from the minimum value where $k_{600} = k_{max}$. As the abrasive distributions become similar, i.e., the overlap decreases, R_s^{600} will have bounding values at high and low concentrations of similar magnitude and become in essence constant or have an extremely shallow slope. This represents the insensitivity the roughness of the smaller abrasive would have due to domination by the larger abrasive in the load bearing contacts. Though, as the distribution overlap decreases, an effect on R_s^{400} as described above will occur simultaneously due to the changes in abrasive distribution interaction. The two distributions become homogenous as the particle diameters become similar.

The total roughness given by Eq. (1) follows a rule of mixtures based on the mass percentage of the slurry particles for each distribution multiplied by the distribution roughness modeled in Eqs. (5), (6), and (11). The rule of mixtures assumption provides an approximate representation of the roughness, since it is determining an average over a surface, similar to a roughness average calculation. The percent of active abrasive particles, n, is defined by $n = k_{max}/(C/(\rho_{H_2O}/\rho_{SiC}))$, where C is the mass percent of abrasive in the slurry, which was held constant at 15.4%, and ρ_{SiC} is the SiC powder density ($= 3.16$ g/cm^3), and is the relationship used to calculate k_{max}. The active abrasive percentage is taken as

Table 2 Values of model parameters used to generate model results in Fig. 9

Parameter	Symbol	Value	
		$P = 2.3$ kg	$P = 4.1$ kg
F-400 diameter (μm)	ϕ_{400}	15.8	
F-600 diameter (μm)	ϕ_{600}	10.3	
Pressure (kPa)	p	4.9	8.8
Reduced modulus (GPa)	E_r	138	
Maximum concentration	$k_{\max}$	8.5×10^{-7}	1.6×10^{-6}
Interaction critical weight ratio	$\chi|_{\%cr}$	0.4	

a model parameter, which is fit to the experimental data. The percentage of active abrasives is the only parameter, which is variable to the experimental data and the shape of the model curve is generated solely on the assumptions made and described in the model formulation. Table 2 presents the necessary model parameter values to compute the results found in the following section.

5 Discussion

In the following sections, we study the relationship among the parameters of the loading, material removal rate, and surface roughness. We found that the abrasive distribution has significant contribution to the outcomes of lapping operation, as shown in Secs. 3 and 4. In this section, the normal loading, material removal rate, and surface roughness will be compared to each other with different abrasive mixing ratios. Results of the surface roughness will be explained in the context of the mixed abrasive roughness model.

5.1 Loading Versus Material Removal Rate. In Fig. 2, the material removal depth of the wafers in lapping is nearly linear with respect of time during the operation. Therefore, the average material removal rate is defined as the total removal depth divided by the operation time, 30 min, as listed in Table 3.

The results in Table 3 show that higher total loading will result in higher MRR, and the larger abrasive grits will produce higher MRR, as expected. However, the highest MRR happens at the 50% mixing ratio of abrasive grits (Fig. 8). This is consistent with the results presented in Bhavagat et al. [1], although the slurry concentrations were not kept at constant for the mixed and single-sized abrasive slurry in that work. In addition, the increase of material removal rate from the single larger abrasive to the 50% mixed ratio abrasive grits is 44% at the loading of 2.3 kg. However, this increase of material removal rate is only 7.8% at the higher loading of 4.1 kg. This means that the mixed abrasive slurry does not significantly affect the material removal rate under higher loadings. The reason could be due to the breakage of abrasives being more severe at higher loading, resulting in similar abrasive distribution during machining. However, compared to lower loading, the higher loading always results in higher material removal rate with the same abrasive mixing ratio.

5.2 Loading Versus Surface Roughness. Table 4 shows the root-mean-square surface roughness value of the wafer surfaces after lapping. From the results, we find that the surface roughness is not dependent on the loading which has been discussed [14,15].
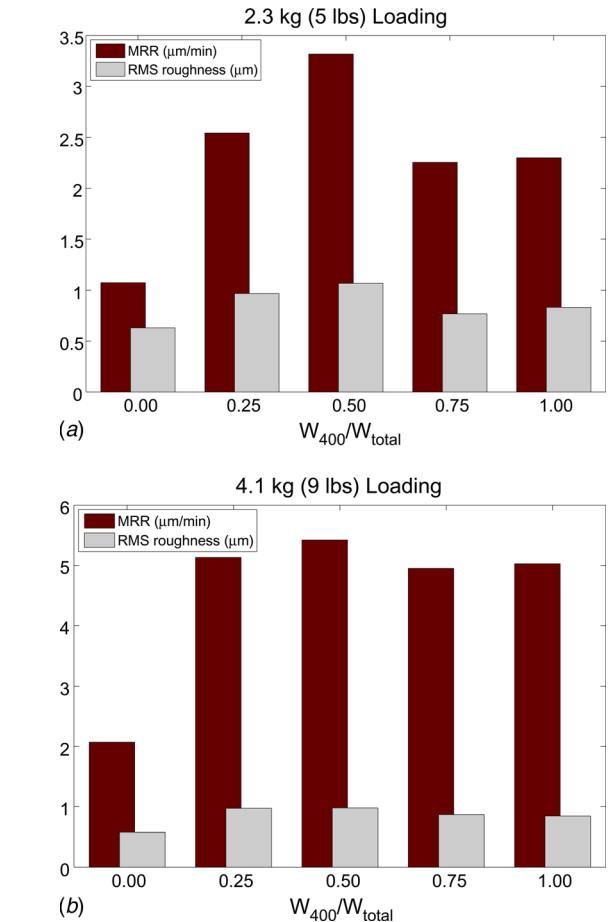

Fig. 8 Comparison of material removal rate and rms surface roughness at (a) 2.3-kg and (b) 4.1-kg loadings

Normally, abrasive grits with smaller mean size produce a smoother surface, and larger abrasives produce a rougher surface finish. In the case of mixed abrasive grits, however, it is obvious that the 50% abrasive mixing ratio produces the surface with the highest roughness. In addition, the abrasive distribution affects the surface roughness. Based on the observation from experiments, the surface roughness of wafers lapped by the mixed abrasives is similar quantitatively to the roughness produced by the slurry with single large abrasives. With higher loading at 4.1 kg, the surface roughness with mixed abrasive ratios 0.25, 0.5, and 0.75 have less variation (see Fig. 4), as compared with the variation under lighter loading. This variation is also observed in the material removal rates in Fig. 8. Figure 9(b) shows a comparison between the model curve (based on Eqs. (1), (5), (6), and (11)) and the experimental roughness measured for a load of 4.1 kg. Here, $n = 3.29 \times 10^{-5}$ and is on a similar order to active particle percentages found by other lapping models [17]. Starting at a low concentration of F-400 (and large concentration F-600) the model predicts a roughness which rises to a maximum value at $\sim 40\% k_{\max}$ and decreases at a lower rate to a roughness value associated with a high concentration of F-400 and low concentration of F-600 particles. The peak occurs due to the individual

Table 3 The average material removal rate (micrometer per minute) under differing loadings and mixing ratios

	$\frac{W_{400}}{W_{total}} = 0$	0.25	0.50	0.75	1
2.3 kg (5 lbs)	1.072	2.544	3.317	2.256	2.300
4.1 kg (9 lbs)	2.072	5.133	5.422	4.950	5.028

Table 4 The average rms surface roughness (micrometer) under differing loadings and mixing ratios

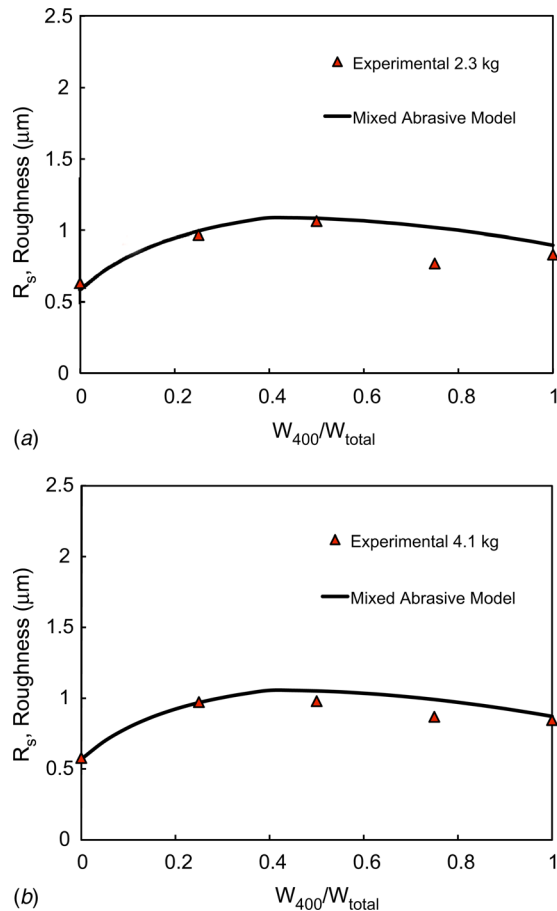|	$\frac{W_{400}}{W_{total}} = 0$	0.25	0.50	0.75	1
2.3 kg (5 lbs)	0.6313	0.9688	1.0646	0.7688	0.8318
4.1 kg (9 lbs)	0.5771	0.9729	0.9792	0.8688	0.8458

Fig. 9 Plot of the mixed abrasive model and the experimentally measured roughness as a function of F-400 particle concentration for (a) 2.3-kg and (b) 4.1-kg cases

distributions having the opposite effect on roughness as a function of the concentration. As the normal load is changed, the roughness is found to have a small increase (Fig. 9) for a decreasing load (from 4.1 to 2.3 kg), resulting in a change in the active abrasive percentage from 3.29×10^{-5} to 1.75×10^{-5} after fitting with the experimental data. The decrease in the active abrasives occurs due to fewer large particles in the distribution becoming trapped between the platen and wafer resulting in less particles actively contributing to roughness generation by sliding contact. With fewer active particles, the load bearing on the active particles increases, which increases the particle penetration, and hence the roughness parameter. The slurry with single small abrasives seems to have much lower surface roughness comparing to those mixed with big abrasives.

5.3 Material Removal Rate Versus Surface Roughness. Figure 8 shows material removal rate and surface roughness in the same figure. From the results of this study, it is obvious that the mixed abrasives with the ratio of $W_{400}/W_{total} = 0.5$ has the highest material removal rate, and also with the highest surface roughness. The slurry with only F-600 abrasive grits has the lowest material removal rate, but the best surface quality. These two figures also show that higher material removal rate comes with the consequence of higher surface roughness in the free abrasive machining process under the same loading.

The material removal rate follows for the most part a Prestonian relationship [30], where the MRR is proportional to the applied pressure, or load. What the Prestonian relationship does not consider is the interaction of the mixed abrasive particle distributions. Here, the MRR follows a near identical trend as was observed for the wafer surface roughness after lapping. Choi et al.

Table 5 The increases of MRR and rms surface roughness from pure F-600 and F-400 to 1:1 mixed abrasive slurries

		MRR (%)	Roughness (%)
2.3 kg	F-600 verus mixed(1:1)	209	69
	F-400 versus mixed	44	28
4.1 kg	F-600 versus mixed	62	70
	F-400 versus mixed	7.8	15

[31] observed similar changes in the MRR as a function of particle size. Though those authors were only considering a single abrasive distribution, for increasing particle diameter a higher MRR was observed. This is effectively the relationship observed in Fig. 8, where as a higher concentration of F-400 particles are added, the MRR increases. The continued increase of the MRR, which begins to decrease (Fig. 8(a)) or actually level-off (Fig. 8(b)) after the 1:1 mixing ratio can be caused by the initiation of rolling-sliding contact with an increase in the percent solids, i.e., particle concentration [31]. The roughness model presented in this paper predicts a larger number of active abrasives for the higher load (4.1 kg) case, which will in turn create more contact points for material removal to occur, leading to an increased MRR at higher loads.

The main objectives of wafer lapping are to remove the layer of subsurface damage due to slicing and global planarization. It is of interest in the lapping process to have large MRR to save process time. Slight increase in surface roughness can be taken care of in the subsequent polishing processes, as long as further subsurface damage is not introduced. From Table 5, we found that MRR is increased with 1:1 mixing ratio, especially for the 2.3 kg loading. This increase of MRR observed in experiments is explained by the proposed model through the interaction of abrasive grits of two different sizes.

Overall, the mixed abrasive slurry performs in a similar manner to the single larger abrasive grit in both material removal and surface roughness. The slurry with the single smaller abrasive, on the other hand, performs differently from the others, indicating that any addition of F-400 particles will alter the material removal rate. Furthermore, the 1:1 mixing ratio removed more material, but resulted in a slightly higher surface roughness, due to interaction between two grades of abrasive grits.

6 Conclusions

In this study, two different sizes of abrasive grits, F-400 and F-600, are mixed in five different ratios to conduct an experimental study on mixed abrasive slurries in the lapping processes. A model based on the Hertzian contact is used to explain the changes of surface roughness resulting from different abrasive mixing ratios. The results show that maximum material removal was achieved at the one-to-one (1:1) abrasive mixing ratio, accompanied by a slightly higher surface roughness than other mixing ratios. Heavier loads always result in higher material removal rates regardless of the abrasive mixing ratios following a Prestonian relationship for material removal. However, the surface roughness does not correlate to the normal load in a significant way. The surface roughness and material removal rate were found to be dependent on the abrasive mixing ratios. To consider the effect of mixed abrasives, the interaction between abrasive sizes was integrated into a contact-based model that explained the trends as a function of mixing ratios and applied load. A critical concentration of the abrasives, $k^* = 0.4\ k_{max}$, was determined as the point where the smaller abrasives began to bear load and affect the surface roughness. Although the reduction of surface roughness is one of the main purposes in lapping, the removal of subsurface damage by quickly and efficiently taking down a layer of material is also important. The results in this study show a potential way of increasing the material removal rate for the coarse lapping process.

Acknowledgment

Nomenclature

R_s = total surface roughness
R_s^{400} = roughness due to F-600 particle distribution
R_s^{600} = roughness due to F-400 particle distribution
χ = weight percent ratio of F-400
ϕ = particle diameter
P = nominal pressure per particle
K = concentration of particles in contact
K_{max} = maximum particle concentration factor
E_r = reduced modulus
$R_{s,\text{limi}}$ = geometric limit to roughness
$R_s^{400}|_{\text{limit}}$ = penetration depth limit of F-400 particles
ϕ_{400} = diameter of F-400 particles
ϕ_{600} = diameter of F-600 particles
ϕ_{400}^{eff} = effective diameter parameter of F-400 particles
ϕ_{600}^{eff} = effective diameter parameter of F-600 particles
β = shift in F-400 particle concentration
k_{400} = concentration of the F-400 particles
k_{600} = concentration of the F-600 particles
$k*$ = critical concentration of F-600 particles in R_s^{400}
$\chi|_{\%\text{cr}}$ = weight percent ratio of F-400 at a given particle percentage related to interaction effect
$\%$cr = ratio of F-600 particles for $\phi_{600} > 15.8 \ \mu$m to the total number of particles in contact
α = ratio of the number of critical F-600 particles which could be in contact
N = percentage of load bearing abrasive particles

References

[1] Bhagavat, S., Liberato, J. C., Chung, C., and Kao, I., 2010, "Effects of Mixed Abrasive Grits in Slurries on Free Abrasive Machining (FAM) Processes," Int. J. Mach. Tools Manuf., **50**, pp. 843–847.
[2] ITRS, 2005, International Technology Roadmap for Semiconductors 2005 edition, Website: http://www.itrs.net/.
[3] Singer, P., 2005, "Is the Industry Ready for 450 mm Wafers?," Semicond. Int., **28**(3), pp. 15.
[4] Pettinato, J. S., and Pillai, D., 2005, "Technology Decisions to Minimize 450-mm Wafer Size Transition Risk," IEEE Trans. Semicond. Manuf., **18**(4), pp. 501–509.
[5] Draina, J., Fandel, D., Ferrell, J., and Kramer, S., 2006, "Lessons Learned From the 300 mm Transition," ECS Trans., **2**(2), pp. 135–154.
[6] Watanabe, M., and Kramer, S., 2006, "450 mm Silicon: An Opportunity and Wafer Scaling," Electrochem. Soc. Interface, **15**(4), pp. 28–31.
[7] Chien, C., Wang, J. K., Chang, T., and Wu, W., 2007, "Economic Analysis of 450mm Wafer Migration," *IEEE International Symposium on Semiconductor Manufacturing Conference Proceedings, 2007 International Symposium on Semiconductor Manufacturing, ISSM–Conference Proceedings*, pp. 283–286.
[8] Hand, A., 2007, "Ismi Updates Goals, Challenges of 450 mm Wafers," Semicond. Int., **30**(1), p. 24.
[9] Intel News Release, 2008, Intel, Samsung Electronics, TSMC reach agreement for 450 mm wafer manufacturing transition. Website: http://www.intel.com/pressroom/archive/releases/2008/20080505corp.htm.
[10] Chung, C., and Kao, I., 2008, "Comparison of Free Abrasive Machining Processes in Wafer Manufacturing," ASME International Conference on Manufacturing Science and Engineering (MSEC 2008), no. ASME Paper No. MSEC2008-72253, ASME.
[11] Yang, F., and Kao, I., 2001. "Free Abrasive Machining in Slicing Brittle Materials With Wiresaw," J. Electron. Packag., **123**, pp. 254–259.
[12] Bhagavat, S., and Kao, I., 2006, "Ultra-Low Load Multiple Indentation Response of Materials: In Purview of Wiresaw Slicing and Other Free Abrasive Machining (FAM) Processes," Int. J. Mach. Tools Manuf., **46**(5), pp. 531–541.
[13] Lawn, B., 1993, *Fracture of Brittle Solids–Second Edition*, Cambridge University Press, Cambridge, United Kingdom.
[14] Phillips, K., Crimes, G. M., and Wilshaw, T. R., 1977, "On the Mechanism of Material Removal by Free Abrasive Grinding Of Glass and Fused Silica," Wear, **41**, pp. 327–350.
[15] Buijs, M., and Houten, K. K., 1993, "Three-Body Abrasion of Brittle Materials as Studied by Lapping," Wear, **166**, pp. 237–245.
[16] Buijs, M., and Houten, K. K., 1993, "A Model for Lapping of Glass," J. Mater. Sci., **28**, pp. 3014–3020.
[17] Chauhan, R., Ahn, Y., Chandrasekar, S., and Farris, T. N., 1993, "Role of Indentation Fracture in Free Abrasive Machining of Ceramics," Wear, **162–164**, pp. 246–257.
[18] Chang, Y. P., Hashimura, M., and Dornfeld, D. A., 2000, "An Investigation of Material Removal Mechanisms in Lapping With Grain Size Transition," J. Manuf. Sci. Eng., **122**, pp. 413–419.
[19] Heisel, U., and Avroutine, J., 2001, "Process Analysis for the Evaluation of the Surface Formation and Removal Rate in Lapping," CIRP Ann., **50**(1), pp. 229–232.
[20] Marinescu, I. D., Uhlmann, E., and Doi, T. K., eds., 2007, *Handbook of Lapping and Polishing*, CRC Press, FL.
[21] Bifano, T., Dow, T., and Scattergood, R., 1991, "Ductile-Regime Grinding: A New Technology for Machining of Brittle Materials," J. Eng. Ind., **113**, pp. 184–189.
[22] Liu, W., Pei, Z. J., and Xin, X. J., 2002, "Finite Element Analysis for Grinding and Lapping of Wire-Sawn Silicon Wafers," J. Mater. Process. Technol., **129**(1–3), pp. 2–9.
[23] Pei, Z. J., Fisher, G. R., and Liu, J., 2008, "Grinding of Silicon Wafers: A Review From Historical Perspectives," Int. J. Mach. Tools Manuf., **48**, pp. 1297–1307.
[24] Li, Z., Pei, Z., and Fisher, G. R., 2006, "Simultaneous Double Side Grinding of Silicon Wafers: A Literature Review," Int. J. Mach. Tools Manuf., **46**, pp. 1449–1458.
[25] Brown, N. J., Baker, P. C., and Maney, R. T., 1981, "Optical Polishing of Metals," Proc. SPIE, **306**, pp. 42–57.
[26] Cook, L. M., 1990, "Chemical Processes in Glass Polishing," J. Non-Cryst. Solids, **120**, pp. 152–171.
[27] Imanaka, O., 1966, "Lapping Mechanics of Glass—Especially on Roughness of Lapped Surface," CIRP Ann., **13**, pp. 227–233.
[28] Wang, C., Sherman, P., Chandra, A., and Dornfeld, D., 2005, "Pad Surface Roughness and Slurry Particle Size Distribution Effects on Material Removal Rate in Chemical Mechanical Planarization," CIRP Ann., **54**, pp. 309–312.
[29] Kao, I., 2004, "Technology and Research of Slurry Wiresaw Manufacturing Systems in Wafer Slicing With Free Abrasive Machining," Int. J. Adv. Manuf. Syst. (IJMAS), Spec Issue Decis. Eng., **7**(2), pp. 7–20.
[30] Preston, F. W., 1927, "The Theory and Design of Plate Glass Polishing Machines," J. Soc. Glass Technol., **11**, pp. 214–256.
[31] Choi, W., Abiade, J., Lee, S.-M., and Singh, R., 2004, "Effects of Slurry Particles on Silicon Dioxide CMP," J. Electrochem. Soc., **151**(8), pp. G512–G522.